Ceramics International 44 (2018) 18123–18128

Contents lists available at ScienceDirect

Ceramics International

journal homepage: www.elsevier.com/locate/ceramint

Low toxicity antisolvent synthesis of composition-tunable luminescent all-inorganic perovskite nanocrystals

Wen Li[a], Wen Deng[a], Xiaoqiang Fan[a], Fengjun Chun[a], Meilin Xie[a], Chao Luo[a], Shiyu Yang[a], Hanan Osman[a], Chuanqi Liu[b], Xiaotong Zheng[a], Weiqing Yang[a,*]

[a] Key Laboratory of Advanced Technologies of Materials (Ministry of Education), School of Materials Science and Engineering, Southwest Jiaotong University, Chengdu 610031, China
[b] College of Optoelectronic Technology, Chengdu University of Information Technology, Chengdu 610225, China

ARTICLE INFO

Keywords:
Perovskite nanocrystals
Low toxicity antisolvent synthesis
Composition dependent luminescent
Phase transformation

ABSTRACT

All-inorganic perovskite nanocrystals have held great promise as incredibly effective luminescent materials and also have been synthesized efficiently by room temperature approaches. Toluene, a high toxicity solvent, is often used as a valid antisolvent in ligand-assisted reprecipitation strategy, which badly restricts the commercial application of this convenient method. Here, aiming to address the toluene toxicity issue, the low toxic tetraethyl orthosilicate (TEOS) is employed as a new alternative antisolvent to achieve high uniform and composition dependent luminescent all-inorganic perovskite Cs_4PbX_6 (X = I, Br, Cl) combined with $CsPbX_3$ (X = I, Br, Cl) nanocrystals with tunable emission large-span wavelengths (626–437 nm) and remarkably narrow full width at half-maximum (FWHM) monochromaticity (down to 19 nm). Meanwhile, the ratio of CsBr to $PbBr_2$ is proved to be a critical factor to control the crystalline phase of the resulting perovskite nanocrystals. Additionally, one monochromatic light-emitting diode (LED) lamp with brightly pure green emission is fabricated based on bromine-based perovskite nanocrystals. This newly developed low toxicity antisolvent synthesis (LTaS) is suitable candidate for commercial production in an environmentally-friendly way, and the as-obtained perovskite materials with superior optical merits will be brought to the forefront of lighting and displays.

1. Introduction

Perovskites as leading candidates for optoelectronic devices exhibit intriguing semiconductor properties by virtue of long charge carrier diffusion lengths, high carrier mobility and long carrier life [1–6]. Depending on their impressive optoelectronic properties, perovskites have attracted considerable attention and also have been explored for potential applications in solar cells [7,8], light emitting diodes (LED) [9,10], photodetectors [11,12] and lasers [13,14]. Particularly organic-inorganic hybrid perovskite solar cells have recorded efficiency higher than 21% recently [15], however, the inherent instability of these hybrid perovskites hinders the scaled production for practical applications [16–19]. Comparatively, Cs-based all-inorganic perovskites demonstrate superior physicochemical performance, especially including low trap state density, higher stability and versatile photoluminescence properties [20–22]. Protesescu et al. first reported the $CsPbX_3$ (X = I, Br, Cl) nanocrystals via the hot-injection method, showing around 90% photoluminescence quantum yield (PLQY) as well as narrow emission peaks and wide color gamut since 2015 [23]. Subsequently, Li et al. introduced a novel supersaturated recrystallization synthesis operated at room temperature, the obtained $CsPbX_3$ (X = I, Br, Cl) quantum dots are comparable with that synthesized by hot-injection method [24]. Taking advantage of ligand density control of quantum dots, Li et al. balanced surface passivation and carrier injection in $CsPbX_3$ LED with a highest external quantum efficiency (EQE) of 6.27% [25]. Hence, emerging all-inorganic perovskite as a new emitter material will fill the impending demand on photoelectric devices, suggesting a luminous future for all-inorganic perovskite LED should be predictable.

Up to now, in order to satisfy the requirements of low cost and large scale production, facile room temperature method is widely employed for the preparation of all inorganic perovskites, which don't need relatively high reaction temperature, inert atmosphere and complex equipment. Sun et al. reported a ligand-mediated reprecipitation strategy accompanied with antisolvent, such as toluene and hexane, and the choice of organic acid and organic amine is critical for systematically manipulating the shape of $CsPbX_3$ colloidal nanocrystals [26]. Recently, Chen et al. demonstrated hexagonal Cs_4PbBr_6 synthesized by an inhomogeneous interface reaction at room temperature,

* Corresponding author.
E-mail address: wqyang@swjtu.edu.cn (W. Yang).

https://doi.org/10.1016/j.ceramint.2018.07.018
Received 20 June 2018; Received in revised form 2 July 2018; Accepted 2 July 2018
Available online 03 July 2018

which exhibited bright green emission with a large binding energy of 222 meV [27]. Analogously, tetragonal $CsPb_2Br_5$ also has been successfully prepared by an alkyl-thiol ligand-assistant method at an ambient condition, and toluene is necessary for the formation of $CsPb_2Br_5$ nanocrystals, which reflected high resistance to high temperature and high humidity environments [28]. For deeper understanding on intrinsic properties of perovskites with different dimensionalities, zero-dimensional Cs_4PbBr_6, two-dimensional $CsPb_2Br_5$ and three-dimensional $CsPbBr_3$ nanocrystals were achieved by a reverse microemulsion method at room temperature, and the phase transformation is triggered by cesium to lead ratio [29]. Generally, dimensionality refers to arrangement of lead halide octahedra in the perovskite crystal, the connectivity of lead halide octahedra dictates the optical behavior of perovskite materials, Pb^{2+} and X^- ions are related to the density of states in conduction and valance band respectively [30]. Although three perovskite-related phases can be obtained by simple room temperature method, most of the previous studies are limited to toluene and hexane as antisolvent, little other environmentally friendly antisolvent has been explored so far.

Herein, we developed a novel low toxicity antisolvent synthesis (LTaS) based on tetraethyl orthosilicate (TEOS) to obtain all-inorganic perovskite naocrystals at room temperature. Due to the low polarity of TEOS, the as-obtained all-inorganic perovskite nanocrystals presented excellently tunable large-span emission wavelengths (626–437 nm) and remarkable monochromaticity with narrow full width at half-maximum (FWHM) (low to 19 nm). Based on it, one typical monochromatic light-emitting diode (LED) lamp with brightly pure green emission was fabricated by employing UV LED chip (centered at 365 nm), evidently suggesting that the prepared perovskite nanocrystals with superior optical merits can be promisingly applied for lighting and also explored displays, and that this LTaS method should dramatically promote the commercial production of all-inorganic perovskite nanocrystals in an environmentally way.

2. Experiment section

2.1. Materials and chemicals

Lead (II) iodide (PbI_2, 99.9%, aladdin), lead (II) bromide ($PbBr_2$, 99.9%, aladdin), lead (II) chloride ($PbCl_2$, 99.9%, aladdin), cesium (I) iodide (CsI, 99.9%, aladdin), cesium (I) bromide (CsBr, 99.9%, aladdin), cesium (I) chloride (CsCl, 99.9%, aladdin), oleylamine (OAm, 80–90%, aladdin), dimethylformamide (DMF, 99.8%, kelong), tetraethyl orthosilicate (TEOS, 99.8%, kelong).

2.2. Synthesis of perovskite nanocrystals

All the reagents were used directly without further purification. In a typical synthesis of green perovskite nanocrystals, 0.4 mmol CsBr and 0.4 mmol $PbBr_2$ were dissolved in 10 mL DMF. 1 mL OA and 0.5 mL OAm were loaded into the precursor solution, and the mixture was magnetically stirred. Then, 1 mL of the precursor solution was quickly transferred into 10 mL TEOS under vigorous stirring. Finally, strong green emission was observed immediately after the precursor was injected into TEOS. Other samples with different emission colors were prepared with the other mixture of PbX_2 and CsX (X = I, Br, Cl). Note that all experimental operations in this paper were implemented in the open air. In addition, the ratios of CsBr to $PbBr_2$ in precursor solution were adjusted as 1:0.33, 1:1, 1:3, 1:5, 1:7 and 1:9, aiming at the transformation of perovskite phase.

2.3. Construction of green LED lamp

First, green perovskite powders were dispersed in a small volume of A glue of silicone for 1 h to ensure fine dispersion of the perovskite nanocrystals. Then, the former mixture was added to a large volume of B glue of silicone (A:B = 1:4 wt%), after stirring the mixture for 20 min, nanocrystals/silicone composite was vacuumed to discharge air bubbles. Subsequently, the mixture was casted onto the surface of a UV LED chip (centered at 365 nm), the sample was dried at 60 °C for 40 min to mix the composite thoroughly. Finally, the temperature was increased to 135 °C to cure the nanocrystals/silicone composite and improve the anti-fading effect, and a monochromatic green LED lamp was obtained by the above procedure.

2.4. Characterization

Powder x-ray diffraction (XRD) was performed using a Bruker D8 Advance x-ray diffractometer using Cu Kα radiation (1.54 Å). Transmission electron microscopy (TEM) study was carried out using a JEOL JEM 2100F field emission transmission electron microscope at 200 kV. Steady state photoluminescence (PL) spectra were acquired using FLS 980 (Edinburgh Instruments).

3. Results and discussion

In this work, LTaS approach was utilized to synthesize perovskite material and the schematic illustration of the detailed formation process and mechanism are illustrated in Fig. 1a. Taking bromine-based perovskite as an example, DMF as a good solvent was used to dissolve CsBr and $PbBr_2$, and the addition of OA and OAm served to control the size and crystal structure of perovskite nanocrystals. Then, TEOS was exploited as a new antisolvent when halides precursor solution was injected into TEOS, the precursors promptly recrystallized and a fluorescent solution was rapidly observed due to different solubility for halides precursor in two solvents. Generally, TEOS is used as silicon source to form SiO_2 to enhance the stability of perovskites [31,32]. Here, by virtue of the symmetry of molecular structure of TEOS, the low polarity as a solvent can facilitate the formation of a supersaturated condition to form the perovskite nanocrystals. TEM image in Fig. 2b obviously reveal well-proportioned perovskite nanocrystals with the size of around 12 nm. After centrifugation, the as-collected yellow powders displayed pure green emission exposured to UV lamp. As toluene was substituted by TEOS, the room temperature synthetic process is not only green safety but also favorable to scale-up trial. In the latter section of this paper, the optical properties and structural features of the all inorganic perovskite materials prepared by this method will be described in detail.

To validate experimentally the suitability of new antisolvent for perovskite in the visible range, we proceeded with the fabrication of mixed halide perovskite. In Fig. 2a, TEOS as antisolvent, a great quantity of the mixed halide perovskite powders were collected, which emitted a variety of colors extending the entire visible region. XRD measurement was directly used to evaluate the phase composition of the mixed halide perovskite samples. The corresponding XRD patterns of as-synthesized mixed halide perovskite powders are presented in Fig. 2b and compared with patterns from standard Cs_4PbBr_6 (JCPDS Card No. 73-2478) and $CsPbCl_3$ (JCPDS Card No. 18-0366). When the ratio of CsBr to $PbBr_2$ was about one, the diffraction peaks were well matched the patterns of standard Cs_4PbBr_6. In a wide range of composition, when Br (1.14 Å) atoms were substituted by bigger I atoms (1.33 Å), leading to an evident blue shift of main diffraction peaks. Conversely, interchanged by smaller Cl (0.99 Å) atoms partially, red shift of the diffraction angles was observed. When the ratio of CsCl to $PbBr_2$ was about one, small shoulder peaks at 21.8°, 31.3° and 38.3° could be indexed to the (101), (200) and (112) planes according to the pattern of standard $CsPbCl_3$. This tendency became more obvious as the Cl content continues rising by changing the precursor, $CsPbX_3$ is the main crystal structure, where the relative intensity of diffractions peaks from $CsPbX_3$ phase to Cs_4PbX_6 phase increased when the ratio of CsBr to $PbCl_2$ was one. XRD analysis indicated that the Cl-rich reaction conditions favor the formation of $CsPbX_3$ structure, while Br-rich and I-

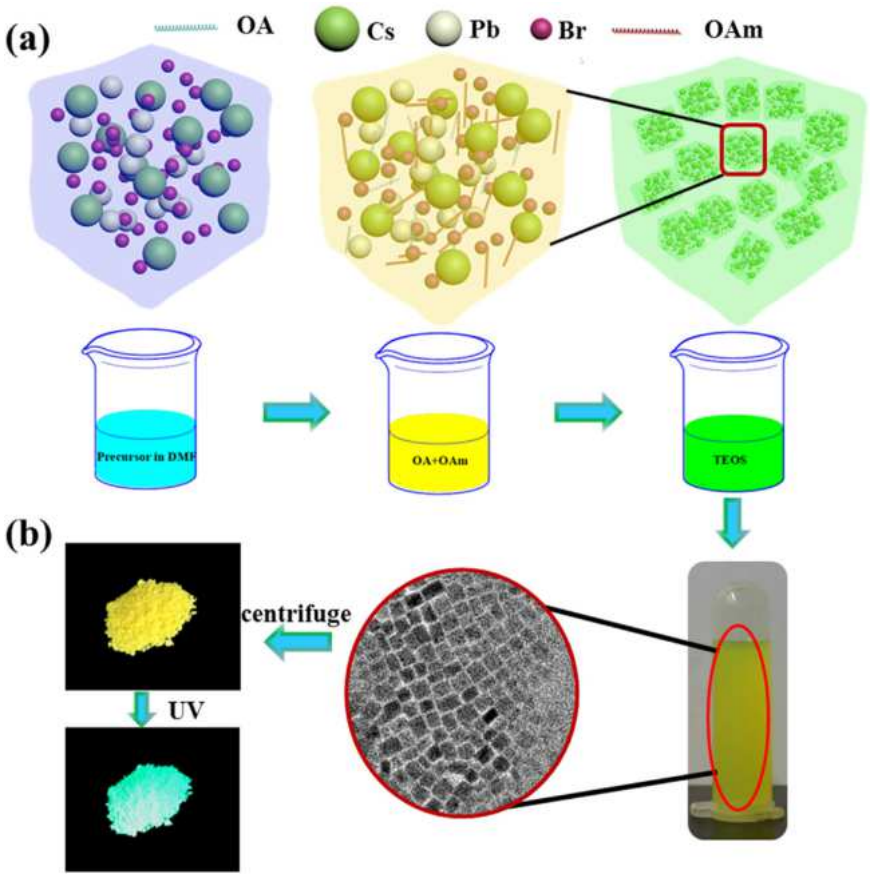

Fig. 1. Perovskite nanocrystals synthesized by LTaS method. (a) Schematic illustration of the formation process. (b) Typical TEM image of perovskite nanocrystals and photographs of perovskite powder and colloid solution.

rich ones tend to form hexagonal Cs_4PbX_6 phase. This regular variation in components and crystal structure of perovskite is dependent on flexible formation of the diverse products attributed to the applicable choice of antisolvent (TEOS).

Fig. 3 showed the representative TEM and HRTEM images of three typical mixed halide perovskite nanocrystals, prepared with $CsBr/PbI_2 = 1$, $CsBr/PbBr_2 = 1$, $CsBr/PbCl_2 = 1$, respectively. In general, the existence of oleylamine and oleic acid as strong binding ligands can control the particle size and shape effectively, and almost monodispersed perovskite nanocrystals were obtained. HRTEM images showed the bright lattice fringes of individual perovskite nanocrystal, and the well-resolved lattice fringes demonstrate the high crystallinity of the halide perovskite nanocrystals. The lattice spacings were calculated to be 0.283 nm and 0.298 nm for I-Br mixed halide samples, which were consistent with the (006) and (223) lattice planes of Cs_4PbX_6 phase. When the ratio of CsBr to $PbCl_2$ was one, the calculated lattice space of 0.301 nm corresponded to (200) lattice plane of Br-Cl mixed halide $CsPbX_3$ nanocrystals in Fig. 3f. These results also evidently

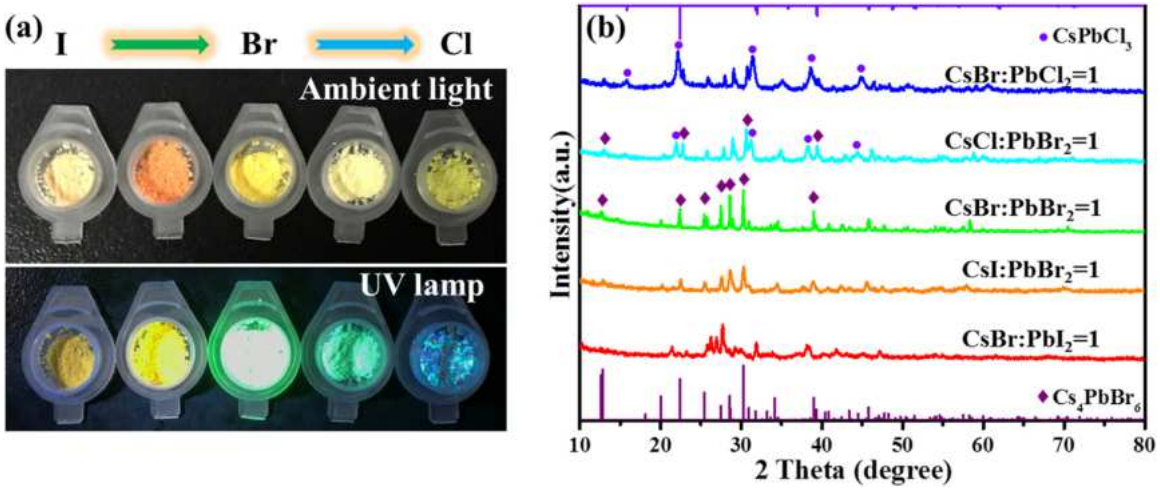

Fig. 2. Structural characterization and photographs of the as-prepared perovskite nanocrystals. (a) Photograph of perovskite powders prepared on a large scale under ambient light and 365 nm UV lamp irradiation. (b) XRD patterns of corresponding perovskite powders.

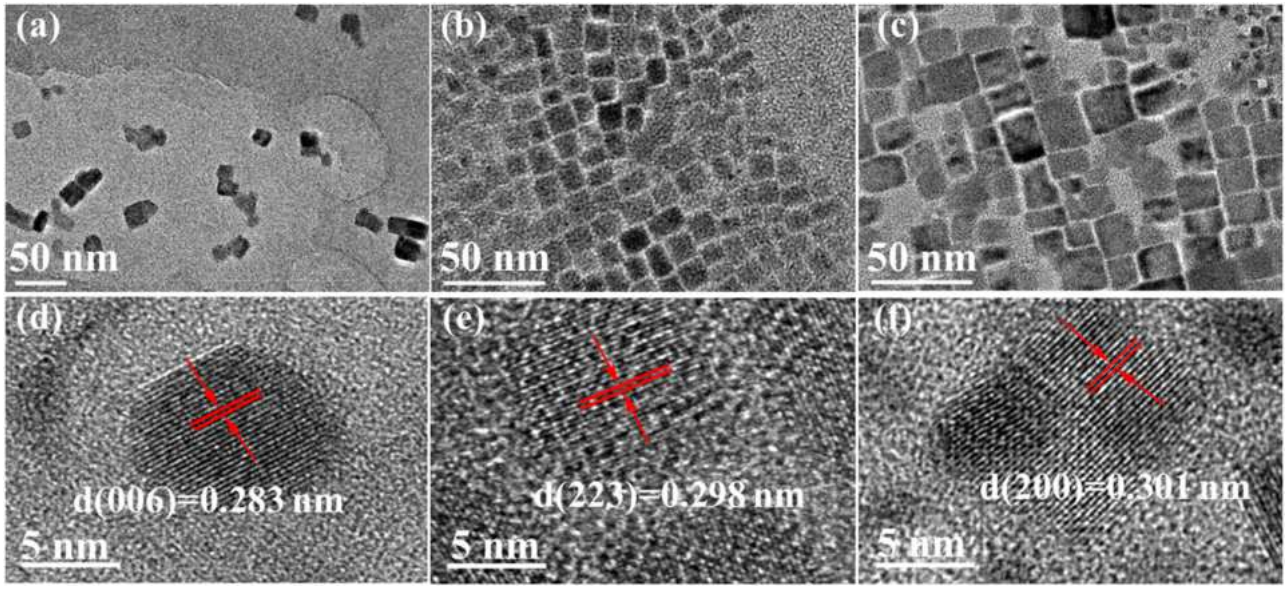

Fig. 3. TEM and HRTEM images of typical perovskite nanocrystals with different precursors. (a, d) CsBr/PbI_2 = 1, (b, e) CsBr/$PbBr_2$ = 1, and (c, f) CsBr/$PbCl_2$ = 1, respectively.

proved that changing halides can achieve high quality and monodispersed nanocrystals with tunable components by the LTaS method.

For the in-depth and comprehensive insight into the luminescent properties of as-prepared perovskite nanocrystals, their emission spectra were investigated and displayed in Fig. 4. By changing the precursors, five typical halide perovskite nanocrystals were obtained which emitted different colors covering visible light range (Fig. 4c). All the samples exhibited a single PL peak, centered at 626 nm, 565 nm, 537 nm, 475 nm and 437 nm, with the emission FWHM of 35 nm, 33 nm, 23 nm, 20 nm and 19 nm, respectively. These narrow FWHM values of PL spectra were definitely beneficial for the fabrication of the monochromatic LEDs with high color purity and high luminous efficiency. In addition, the PL peak demonstrated a remarked blue shift from 626 nm to 437 nm upon the partial replacement of I constituent from Br to Cl, this systematic change caused the variation in the optical gap which made contribution to versatile emission colors. Therefore, as a new and low toxicity antisolvent, TEOS successfully constructed a favorable environment for supersaturated recrystallization to efficiently guarantee the excellent luminescent performance of all-inorganic perovskite nanocrystals.

In order to determinate of fluorescent phase of the as-prepared all inorganic perovskite nanocrystals, we also probed the influence of the ratios of CsBr to $PbBr_2$ on the phase transformation of bromine-based perovskite. XRD patterns were used to determine the phases of the as-obtained perovskite materials. Fig. 5a showed the XRD patterns of the final products with different ratios of CsBr to $PbBr_2$ (1:0.33, 1:1, 1:3, 1:5, 1:7 and 1:9). When the molar ratios of CsBr to $PbBr_2$ are 1:0.33 and 1:1, the XRD patterns were assigned to zero dimensional Cs_4PbBr_6. After decreasing the ratio to 1:3, major peaks of the XRD patterns were labeled to three dimensional $CsPbBr_3$ (JCPDS Card No. 18-0364). When the ratio was further decreased to 1:3 and 1:7, the product was a mixture of $CsPb_2Br_5$ (JCPDS Card No. 25-0211) and $CsPbBr_3$. With the increased $PbBr_2$ and reduced CsBr content, the incorporation of $PbBr_2$ into Cs_4PbBr_6 crystal structure and dissociation of CsBr from $CsPbBr_3$ cause phase transformation [30,33,34]. As the ratio continuously dropped to 1:9, an unreported phase has been discovered. Incredibly, it

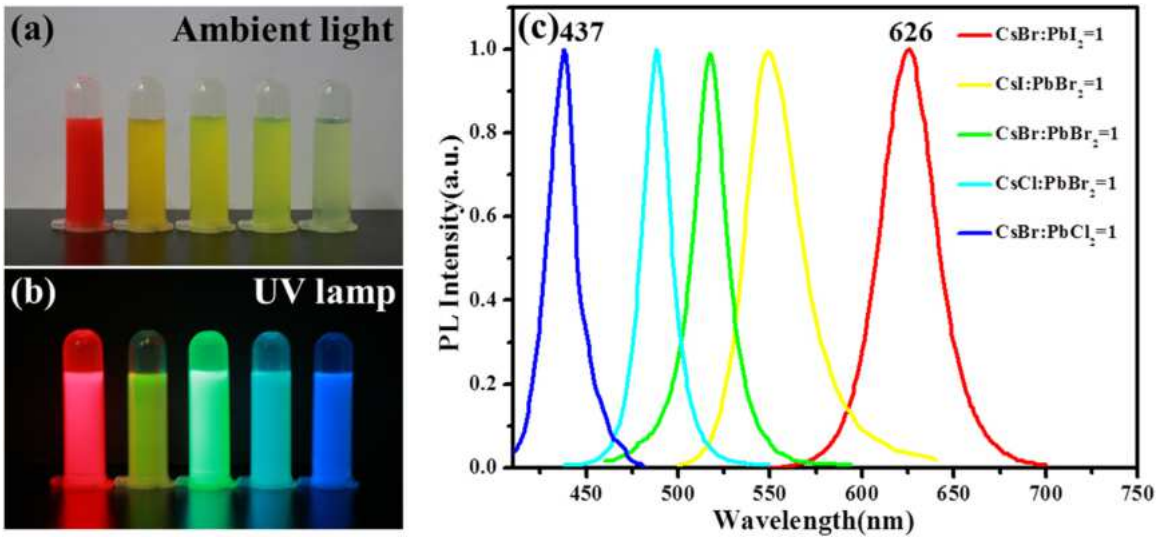

Fig. 4. Optical properties of the as-prepared perovskite nanocrystals. Photographs of all inorganic perovskite nanocrystals in TEOS under (a) ambient light and (b) 365 nm UV lamp irradiation. (c) Photoluminescence spectra of the five typical samples with different component of halides.

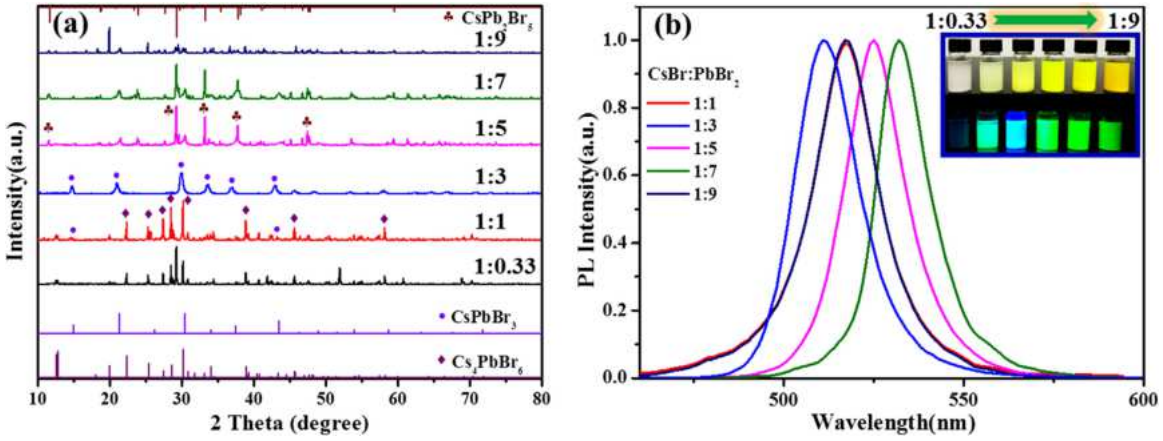

Fig. 5. Structural and luminescent properties of the as-prepared perovskite nanocrystals by controlling the ratios of CsBr to $PbBr_2$. (a) XRD patterns of bromine-based perovskite nanocrystals. (b) Photoluminescence spectra of the corresponding perovskite colloidal solution. Inset showing bromine-based perovskite in TEOS under ambient light and 365 nm UV lamp irradiation.

is difficult to determine the phase composition according to the published reference. The characteristic diffraction peaks of this sample do not belong to impurity phases such as CsBr and $PbBr_2$, and future work will focus on this phenomenon. As presented in Fig. 5b, the photoluminescence spectra of the corresponding perovskite colloidal solution shifted from 510 nm to 532 nm. Recently, Cs_4PbBr_6 as a luminescent material is controversial. Mohammed's group has shown that Cs_4PbBr_6 is highly luminescent with a band gap of 2.33 eV [35,36]. However, a recent work shows that Cs_4PbBr_6 is a non-luminescent material because of high band gap (3.95 eV), and they think that the reported emissive Cs_4PbBr_6 is originated from the presence of $CsPbBr_3$ impurities [30]. Here when the ratio of CsBr to $PbBr_2$ was 1:0.33, the photoluminescence spectra of this sample cannot be measured, which is consistent with the phenomenon shown in the inset of Fig. 5b, confirming that Cs_4PbBr_6 phase is non-fluorescent. For the sample with the ratio of 1:1, Cs_4PbBr_6 crystal structure was the major phase and a few $CsPbBr_3$ nanocrystals may be presented together which emits real fluorescence. In addition, the emission peak of $CsPbBr_3$ has an obvious blue shift than the Cs_4PbBr_6 and $CsPb_2Br_5$, suggesting $CsPbBr_3$ phase has more significant quantum confinement effect than Cs_4PbBr_6 and $CsPb_2Br_5$ phases. In brief, TEOS as an antisolvent can realize the controllable transformation of crystal structure for perovskite.

Finally, in order to explore the practical application of all-inorganic perovskite nanocrystals by using LTaS approach, one monochromatic LED lamp with brightly pure green emission was fabricated as shown in Fig. 6a. This green LED lamp was constructed integrating bromine-based nanocrystals with a commercially available 365 nm GaN LED chip, and this LED lamp can work well even after the thermal treatment at 408 K, certainly indicating these all-inorganic perovskite nanocrystals have promising application in the optoelectronics field against harsh environment. Moreover, the narrow emission spectrum strongly confirmed the good monochromaticity of this green LED lamp with the corresponding color coordinate of (0.2931, 0.6928) (Fig. 6c), unambiguously rendering the potentially commercial possibility of all-inorganic perovskite nanocrystals green-manufactured by LTaS approach.

4. Conclusion

In summary, through the exploitation of TEOS solvent, a low toxicity and suitable antisolvent, we have developed a novel LTaS method to successfully synthetize monodispersed and luminescent all-inorganic perovskite nanocrystals at room temperature. These as-prepared nanocrystals deliver controllably large span emission spectra ranged from 437 nm to 626 nm as well as excellent narrow FWHM (low to 19 nm) monochromaticity. More importantly, only by adjusting the ratios of CsBr to $PbBr_2$, this kind of LTaS approach with TEOS can be used to synthesize bromine-based perovskites with different phase structure, Cs_4PbBr_6, $CsPbBr_3$ and $CsPb_2Br_5$. Besides, a bright green LED lamp by a combination of perovskite nanocrystals and UV LED chip has been packaged for the confirmation of its practical application. Hence, TEOS will be a candidate to substitute toluene and hexane for the syntheses of perovskite materials. We believe that this study will pave the way to green-exploit the various all inorganic perovskite materials, and further expand the applications for all-inorganic perovskites, like color converters and LEDs.

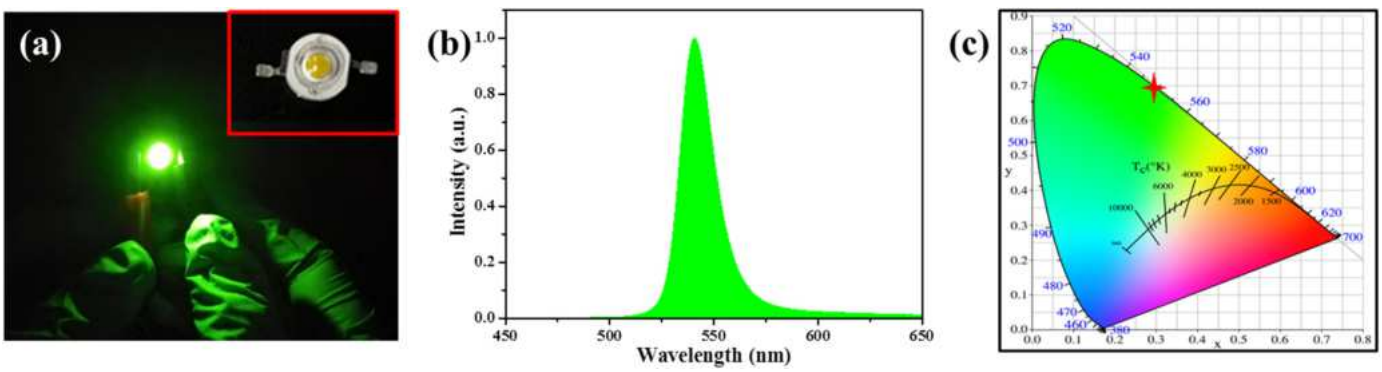

Fig. 6. The spectra characteristics of bromine-based perovskite nanocrystals based LED lamp. (a) The picture of green LED lamp. (b) PL emission spectrum and (c) CIE chromaticity coordinate of the green LED lamp.

Acknowledgments

This work is supported by the Scientific and Technological Projects for Distinguished Young Scholars of Sichuan Province (No. 2015JQ0013), the Fundamental Research Funds for the Central Universities of China (A0920502051408-10 and ZYGX2009Z0001).

Data statement

The processed data required to reproduce these findings cannot be shared at this time as the data also forms part of an ongoing study.

References

[1] D. Shi, V. Adinolfi, R. Comin, M.J. Yuan, E. Alarousu, A. Buin, Y. Chen, S. Hoogland, A. Rothenberger, K. Katsiev, Y. Losovyj, X. Zhang, P.A. Dowben, O.F. Mohammed, E.H. Sargent, O.M. Bakr, Low trap-state density and long carrier diffusion in organolead trihalide perovskite single crystals, Science 347 (2015) 519–522.

[2] V.K. Ravi, G.B. Markad, A. Nag, Band edge energies and excitonic transition probabilities of colloidal $CsPbX_3$ (X = Cl, Br, I) perovskite nanocrystals, ACS Energy Lett. 1 (2016) 665–671.

[3] H.Z. Sun, Z.Y. Yang, M.Y. Wei, W. Sun, X.Y. Li, S.Y. Ye, Y.B. Zhao, H.R. Tan, E.L. Kynaston, T.B. Schon, H. Yan, Z.–H. Lu, G.A. Ozin, E.H. Sargent, D.S. Seferos, Chemically addressable perovskite nanocrystals for light-emitting applications, Adv. Mater. 29 (2017) 1701153.

[4] M.C. Weidman, A.J. Goodman, W.A. Tisdale, Colloidal halide perovskite nanoplatelets: an exciting new class of semiconductor nanomaterials, Chem. Mater. 29 (2017) 5019–5030.

[5] M.V. Kovalenko, L. Protesescu, M.I. Bodnarchuk, Properties and potential optoelectronic applications of lead halide perovskite nanocrystals, Science 358 (2017) 745–750.

[6] Q.A. Akkerman, G. Rainò, M.V. Kovalenko, L. Manna, Genesis, challenges and opportunities for colloidal lead halide perovskite nanocrystals, Nat. Mater. 17 (2018) 394–405.

[7] O. Ergen, S.M. Gilbert, T. Pham, S.J. Turner, M.T.Z. Tan, M.A. Worsley, A. Zettl, Graded bandgap perovskite solar cells, Nat. Mater. 16 (2017) 522–525.

[8] Z. Li, T.R. Klein, D.H. Kim, M.J. Yang, J.J. Berry, M.F.A.M. van Hest, K. Zhu, Scalable fabrication of perovskite solar cells, Nat. Rev. Mater. 3 (2018) 18017.

[9] Z.G. Xiao, R.A. Kerner, L.F. Zhao, N.L. Tran, K.M. Lee, T.–W. Koh, G.D. Scholes, B.P. Rand, Efficient perovskite light-emitting diodes featuring nanometre-sized crystallites, Nat. Photonics 11 (2017) 108–115.

[10] M. Abdi-Jalebi, Z. Andaji-Garmaroudi, S. Cacovich, C. Stavrakas, B. Philippe, J.M. Richter, M. Alsari, E.P. Booker, E.M. Hutter, A.J. Pearson, S. Lilliu, T.J. Savenije, H. Rensmo, G. Divitini, C. Ducati, R.H. Friend, S.D. Stranks, Maximising and stabilising luminescence in metal halide perovskite device structures, Nature 555 (2018) 497–501.

[11] X.M. Li, D.J. Yu, J. Chen, Y. Wang, F. Cao, Y. Wei, Y. Wu, L. Wang, Y. Zhu, Z.G. Sun, J.P. Ji, Y.L. Shen, H.D. Sun, H.B. Zeng, Constructing fast carrier tracks into flexible perovskite photodetectors to greatly improve responsivity, ACS Nano 11 (2017) 2015–2023.

[12] L. Dou, Y.M. Yang, J. You, Z. Hong, W.H. Chang, G. Li, Y. Yang, Solution-processed hybrid perovskite photodetectors with high detectivity, Nat. Commun. 5 (2014) 5404.

[13] S.A. Veldhuis, P.P. Boix, N. Yantara, M.J. Li, T.C. Sum, N. Mathews, S.G. Mhaisalkar, Perovskite materials for light-emitting diodes and lasers, Adv. Mater. 28 (2016) 6804–6834.

[14] W.Z. Sun, K.Y. Wang, Z.Y. Gu, S.M. Xiao, Q.H. Song, Tunable perovskite microdisk lasers, Nanoscale 8 (2016) 8717–8721.

[15] D.Q. Bi, C.Y. Yi, J.S. Luo, J.–D. Décoppet, F. Zhang, S.M. Zakeeruddin, X. Li, A. Hagfeldt, M. Grätzel, Polymer-templated nucleation and crystal growth of perovskite films for solar cells with efficiency greater than 21%, Nat. Energy 1 (2016) 16142.

[16] T. Leijtens, K. Bush, R. Cheacharoen, R. Beal, A. Bowring, M.D. McGehee, Towards enabling stable lead halide perovskite solar cells; interplay between structural, environmental, and thermal stability, J. Mater. Chem. A 5 (2017) 11483–11500.

[17] Y. Bai, Q.F. Dong, Y.C. Shao, Y.H. Deng, Q. Wang, L. Shen, D. Wang, W. Wei, J.S. Huang, Enhancing stability and efficiency of perovskite solar cells with crosslinkable silane-functionalized and doped fullerene, Nat. Commun. 7 (2016) 12806.

[18] T.A. Berhe, W.–N. Su, C.–H. Chen, C.–J. Pan, J.–H. Cheng, H.–M. Chen, M.–C. Tsai, L.–Y. Chen, A.A. Dubale, B.–J. Hwang, Organometal halide perovskite solar cells: degradation and stability, Energy Environ. Sci. 9 (2016) 323–356.

[19] T.M. Koh, V. Shanmugam, X.T. Guo, S.S. Lim, O. Filonik, E.M. Herzig, P. Müller-Buschbaum, V. Swamy, S.T. Chien, S.G. Mhaisalkar, N. Mathews, Enhancing moisture tolerance in efficient hybrid 3D/2D perovskite photovoltaics, J. Mater. Chem. A 6 (2018) 2122–2128.

[20] G. Nedelcu, L. Protesescu, S. Yakunin, M.I. Bodnarchuk, M.J. Grotevent, M.V. Kovalenko, Fast anion-exchange in highly luminescent nanocrystals of cesium lead halide perovskites ($CsPbX_3$, X = Cl, Br, I), Nano Lett. 15 (2015) 5635–5640.

[21] S. Ananthakumar, Jeyagopal R. Kumar, S.M. Babu, Cesium lead halide ($CsPbX_3$,X = Cl, Br, I) perovskite quantum dots synthesis, properties, and applications: a review of their present status, J. Photon. Energy 6 (2016) 042001.

[22] X.M. Li, F. Cao, D.J. Yu, J. Chen, Z.G. Sun, Y.L. Shen, Y. Zhu, L. Wang, Y. Wei, Y. Wu, H.B. Zeng, All inorganic halide perovskites nanosystem: synthesis, structural features, optical properties and optoelectronic spplications, Small 13 (2017) 1603996.

[23] L. Protesescu, S. Yakunin, M.I. Bodnarchuk, F. Krieg, R. Caputo, C.H. Hendon, R.X. Yang, A. Walsh, M.V. Kovalenko, Nanocrystals of cesium lead halide perovskites ($CsPbX_3$, X = Cl, Br, and I): novel optoelectronic materials showing bright emission with wide color gamut, Nano Lett. 15 (2015) 3692–3696.

[24] X.M. Li, Y. Wu, S.L. Zhang, B. Cai, Y. Gu, J.Z. Song, H.B. Zeng, Quantum dots: $CsPbX_3$ quantum dots for lighting and displays: room-temperature synthesis, photoluminescence superiorities, underlying origins and white light-emitting diodes, Adv. Funct. Mater. 26 (2016) (2584–2584).

[25] J.H. Li, L.M. Xu, T. Wang, J.Z. Song, J.W. Chen, J. Xue, Y.H. Dong, B. Cai, Q.S. Shan, B.N. Han, H.B. Zeng, 50-Fold EQE improvement up to 6.27% of solution-processed all-inorganic perovskite $CsPbBr_3$ QLEDs via surface ligand density control, Adv. Mater. 29 (2017) 1603885.

[26] S.B. Sun, D. Yuan, Y. Xu, A.F. Wang, Z.T. Deng, Ligand-mediated synthesis of shape-controlled cesium lead halide perovskite nanocrystals via reprecipitation process at room temperature, ACS Nano 10 (2016) 3648–3657.

[27] D.Q. Chen, Z.Y. Wan, X. Chen, Y.J. Yuan, J.S. Zhong, Large-scale room-temperature synthesis and optical properties of perovskite-related Cs_4PbBr_6 fluorophores, J. Mater. Chem. C 4 (2016) 10646–10653.

[28] L.F. Ruan, W. Shen, A.F. Wang, A.S. Xiang, Z.T. Deng, Alkyl-thiol ligand-induced shape- and crystalline phase-controlled synthesis of stable perovskite-related $CsPb_2Br_5$ nanocrystals at room temperature, J. Phys. Chem. Lett. 8 (2017) 3853–3860.

[29] H.Z. Yang, Y.H. Zhang, J. Pan, J. Yin, O.M. Bakr, O.F. Mohammed, Room-temperature engineering of all-inorganic perovskite nanocrsytals with different dimensionalities, Chem. Mater. 29 (2017) 8978–8982.

[30] Q.A. Akkerman, S. Park, E. Radicchi, F. Nunzi, E. Mosconi, F.D. Angelis, R. Brescia, P. Rastogi, M. Prato, L. Manna, Nearly monodisperse insulator Cs_4PbX_6 (X = Cl, Br, I) nanocrystals, their mixed halide compositions, and their transformation into $CsPbX_3$ nanocrystals, Nano Lett. 17 (2017) 1924–1930.

[31] H.–C. Wang, S.–Y. Lin, A.–C. Tang, B.P. Singh, H.–C. Tong, C.–Y. Chen, Y.–C. Lee, T.–L. Tsai, R.–S. Liu, Mesoporous silica particles integrated with all-inorganic $CsPbBr_3$ perovskite quantum-dot nanocomposites (MP-PQDs) with high stability and wide color gamut used for backlight display, Angew. Chem. Int. Ed. 55 (2016) 7924–7929.

[32] H.C. Hu, L.Z. Wu, Y.S. Tan, Q.X. Zhong, M. Chen, Y.H. Qiu, D. Yang, B.Q. Sun, Q. Zhang, Y.D. Yin, Interfacial synthesis of highly stable $CsPbX_3$/oxide janus nanoparticles, J. Am. Chem. Soc. 140 (2017) 406–412.

[33] L.Z. Wu, H.C. Hu, Y. Xu, S. Jiang, M. Chen, Q.X. Zhong, D. Yang, Q.P. Liu, Y. Zhao, B.Q. Sun, Q. Zhang, Y.D. Yin, From nonluminescent Cs_4PbX_6 (X = Cl, Br, I) nanocrystals to highly luminescent $CsPbX_3$ nanocrystals: water-triggered transformation through a CsX-stripping mechanism, Nano Lett. 17 (2017) 5799–5804.

[34] W. Shen, L.F. Ruan, Z.T. Shen, Z.Y. Deng, Reversible light-mediated compositional and structural transitions between $CsPbBr_3$ and $CsPb_2Br_5$ nanosheets, Chem. Commun. 54 (2018) 2804–2807.

[35] Y.H. Zhang, M.I. Saidaminov, I. Dursun, H.Z. Yang, B. Murali, E. Alarousu, E. Yengel, B.A. Alshankiti, O.M. Bakr, O.F. Mohammed, Zero-dimensional Cs_4PbBr_6 perovskite nanocrystals, J. Phys. Chem. Lett. 8 (2017) 961–965.

[36] M.I. Saidaminov, J. Almutlaq, S. Sarmah, I. Dursun, A.A. Zhumekenov, R. Begum, J. Pan, N. Cho, O.F. Mohammed, O.M. Bakr, Pure Cs_4PbBr_6: highly luminescent zero-dimensional perovskite solids, ACS Energy Lett. 1 (2016) 840–845.